Biol Cybern (2012) 106:27–36
DOI 10.1007/s00422-012-0479-5

ORIGINAL PAPER

Biological Cybernetics

Unlearning tinnitus-related cerebral synchrony with acoustic coordinated reset stimulation: theoretical concept and modelling

Peter A. Tass · Oleksandr V. Popovych

Received: 27 October 2009 / Accepted: 26 January 2012 / Published online: 21 February 2012

Abstract Tinnitus is a deafferentation-induced phantom phenomenon characterized by abnormal cerebral synchrony and connectivity. Computationally, we show that desynchronizing acoustic coordinated reset (CR) stimulation can effectively counteract both up-regulated synchrony and connectivity. CR stimulation has initially been developed for the application to electrical deep brain stimulation. We here adapt this approach to non-invasive, acoustic CR stimulation. For this, we use the tonotopic organization of the central auditory system and replace electrical stimulation bursts applied to different brain sites by acoustically delivered tones of different pitch. Based on our simulations, we propose non-invasive acoustic CR stimulation as a possible novel therapy for tinnitus.

Keywords Tinnitus · Coordinated reset · Anti-kindling · Spike timing-dependent plasticity · Multistability

1 Introduction

Millions of people suffer from subjective tinnitus, the sensation of sounds in the absence of any external or internal sound source. In 1% of the population the life quality is seriously impaired by chronic tinnitus (Heller 2003; McFadden 1982). Tinnitus is typically associated with the damage to the peripheral hearing system (Irvine et al. 2001; Weisz et al. 2006) which is followed by a sequence of structural and functional changes in the central hearing system (Eggermont and Roberts 2004). There are relevant similarities between tinnitus and phantom limb pain, the latter being characterized by a reorganization of the primary somatosensory cortex (Elbert et al. 1994; Flor et al. 1995). Tinnitus is, hence, considered as an auditory phantom phenomenon (Jastreboff 1990; Mühlnickel et al. 1998). The reduced or absent afferent cochlear input causes a reorganization of tonotopic cortical maps, where representations of those frequency regions neighbouring the deafferented part become expanded (Calford et al. 1993; Rajan and Irvine 1998). There is a strong positive correlation between tinnitus loudness and the amount of cortical reorganization (Mühlnickel et al. 1998).

In addition, chronic tinnitus is characterized by specific alterations of the spontaneous brain activity: alpha power (8–12 Hz) is reduced, whereas delta (1.5–4 Hz) and gamma powers (>30 Hz) are enhanced, in particular, in the temporal regions (Weisz et al. 2005, 2007). The altered corticothalamic and corticolimbic interactions are considered to cause the enhanced delta rhythm which in turn drives the gamma rhythm (Weisz et al. 2007). Pathologically enhanced delta activity emerges in cortical regions deprived of afferent input (Steriade 2006). There is a tight relationship between tinnitus loudness, on the one hand, and delta power in temporal regions (Dohrmann et al. 2007; Kahlbrock and Weisz 2008) or theta power extradurally recorded from the secondary auditory cortex (De Ridder et al. 2011). While the cortical reorganization evolves on a slow time scale within several days or weeks (Robertson and Irvine 1989), the tinnitus percept and the related neuronal synchronization follow a noise trauma typically immediately (Norena and Eggermont 2003; Ortmann et al. 2011). As pathological neuronal synchronization processes are considered to be the correlate of the tinnitus percept (Dohrmann et al. 2007; Kahlbrock and Weisz 2008;

P. A. Tass (✉) · O. V. Popovych
Institute of Neuroscience and Medicine - Neuromodulation (INM-7), Research Center Jülich, 52425 Jülich, Germany
e-mail: p.tass@fz-juelich.de

P. A. Tass
Department of Stereotaxic and Functional Neurosurgery, University Hospital, 50924 Cologne, Germany

De Ridder et al. 2011), in a first step, we here focus on the control of tinnitus-related pathological synchrony.

In neuronal populations, changes of dynamics and connectivity are intimately connected (Yuste and Bonhoeffer 2004). Spike timing-dependent plasticity (STDP) up- or down-regulates synaptic weights depending on the relative timing of pre- and post-synaptic spikes (Gerstner et al. 1996; Markram et al. 1997). A striking feature of neural and phase oscillator networks with STDP is their multistablility (Tass and Majtanik 2006; Tass and Hauptmann 2007, 2009; Hauptmann and Tass 2007): Different attractors coexist which differ with respect to their fast neuronal dynamics and their slow synaptic dynamics (i.e. connectivity pattern). Stable desynchronized states with weak mean synaptic weight coexist with stable synchronized states with strong mean synaptic weight. As shown numerically, by appropriate stimulation, a network is shifted from one attractor to another, so that the stimulation effects outlast the stimulus offset. In particular, desynchronizing coordinated reset (CR) stimulation (Tass 2003b,a) shifts a network from a synchronized state with strong coupling (i.e. mean synaptic weight) to a desynchronized state with weak coupling (Tass and Majtanik 2006; Tass and Hauptmann 2007, 2009; Hauptmann and Tass 2007). In other words, under CR stimulation the network gets reshaped and unlearns up-regulated synchrony. Long-lasting desynchronization caused by CR stimulation has experimentally been verified in rat hippocampal slice rendered epileptic by magnesium withdrawal (Tass et al. 2009).

We here adapt this CR anti-kindling approach to the case of subjective tonal tinnitus and illustrate our concept by means of simulations. To this end, we first present a simplified model of partially deafferented auditory cortex receiving afferent auditory input and desynchronizing CR stimulation. Finally, we sketch how to transform the concept of electrical CR stimulation, designed for the application to electrical deep brain stimulation (Tass 2003b,a), to a concept of non-invasive, acoustic CR stimulation as a possible treatment of tinnitus.

2 Model

As a simple model for the primary auditory cortex, we consider an ensemble of N interacting neurons receiving an external input (in a first approximation modelling the afferent input from the inner ear) and acoustic CR stimulation. Since many studies underlined the importance of bursting neuronal discharges for pathological neuronal dynamics associated with tinnitus (Bauer et al. 2008; Finlayson and Kaltenbach 2009), we consider a model of bursting neurons. We however expect that the main results revealed below can be obtained for spiking neurons as well. As a model for a single neuron, we use the FitzHugh–Rinzel (FHR) bursting neuron (Rinzel 1987; Izhikevich 2001; Baer and Gaekel 2008). This yields

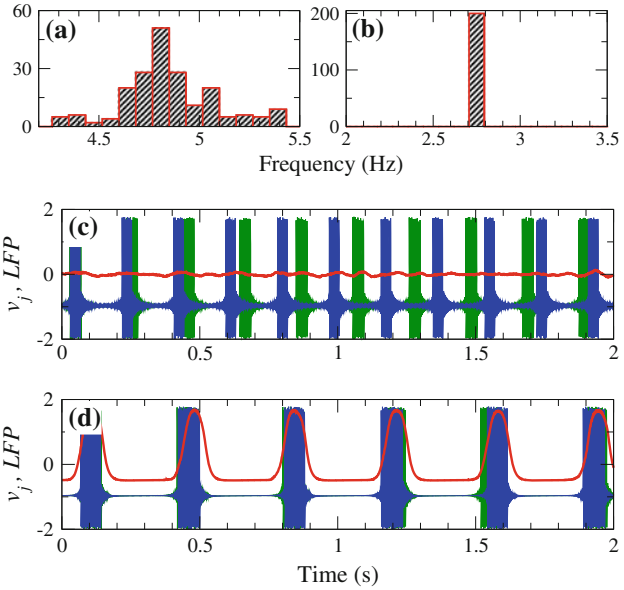

Fig. 1 Dynamics of the neuronal population (1)–(3) without STDP, input and stimulation ($F_i = 0$ in Eq.1). **a**, **b** Histograms of the individual burst frequencies $\{\omega_j\}$ (average number of bursts per time unit). **c**, **d** Membrane potentials v_i of two selected neurons (*green and blue curves*) and DC-balanced local field potential $LFP(t) - \langle LFP(t)\rangle$ (*red curve*, $\langle\cdot\rangle$ denotes time averaging) for two types of connectivity: **a**, **c** $c_{ij} = 0$ (uncoupled neurons) and **b**, **d** $c_{ij} = 0.5$ (strong coupling). LFP is multiplied by 10 to be adapted to the scale of the plots. The constant currents I_i are uniformly randomly distributed in the interval $I_i \in [0.347, 0.353]$. Number of neurons $N = 200$; $\nu = 10$, $\delta = 0.8$, $a = 0.7$, $b = 0.8$, $\mu = 0.001$, $c = -0.9$, $d = 1.0$, $\alpha = 0.08$, $\beta = 0.07$, $\sigma_1 = 3.5$, $\sigma_2 = 2$, and $V_r = 2$

$$\begin{aligned}\dot{v}_i &= \nu(v_i - v_i^3/3 - w_i + y_i + I_i) + S_i(t) + F_i(t),\\ \dot{w}_i &= \delta(a + v_i - bw_i),\\ \dot{y}_i &= \mu(c - v_i - dy_i), \qquad i = 1,\ldots,N.\end{aligned} \tag{1}$$

$S_i(t)$ denotes the internal synaptic interaction, and $F_i(t)$ the external input and stimulation. v_i are the membrane potentials of the individual neurons. The constant currents I_i are uniformly distributed random numbers: $I_i \in [0.347, 0.353]$. Consequently, without synaptic interactions and external input, $S_i(t) = F_i(t) = 0$ in Eq. 1, the mean frequencies ω_i (average number of bursts per time unit) of the FHR neurons (1) are broadly distributed around the mean value $\overline{\omega} \approx 4.85$Hz with standard deviation $\sigma_\omega \approx 0.23$ (Fig. 1a). The individual neurons burst independently of each other (Fig. 1c). With each, burst action potentials reach the post-synaptic neuron and contribute to a post-synaptic potential (PSP) (Gerstner and Kistler 2002; Izhikevich 2007). The PSP $s_i(t)$ generated by the i-th neuron reads (Golomb and Rinzel 1993; Terman et al. 2002)

$$\dot{s}_i = \frac{\alpha}{(1 + \exp(-(v_i + 0.1)/0.25)}(1 - s_i) - \beta s_i. \tag{2}$$

The neurons interact via excitatory and inhibitory (e.g. via interneurons) synapses. The synaptic coupling current $S_i(t)$ in Eq. 1 reads

$$S_i(t) = \frac{1}{N}\sum_{j=1}^{N}(V_{r,ij} - v_i(t)) \cdot |M(i,j)|c_{ij}s_j(t). \quad (3)$$

$C = \{c_{ij}\}$ is the matrix of the synaptic weights c_{ij} of the pre-synaptic neuron j to the post-synaptic neuron i. Function $M(i,j)$ defines the spatial profile of the coupling and has the form of a mexican hat: $M(i,j) = (1 - d_{ij}^2/\sigma_1^2)\exp(-d_{ij}^2/2\sigma_2^2)$, where $d_{ij} = d_0|i-j|$ is the distance between the neurons i and j, and $d_0 = 10/(N-1)$. To avoid boundary effects, we assume that the neuronal fibres are uniformly distributed within the neuronal population such that the distance $|i-j|$ is replaced by $N - |i-j|$, if the indexes i and j get more than $N/2$ apart from each other. The positive (negative) values of $M(i,j)$ indicate an excitatory (inhibitory) interaction, which corresponds to closely (distantly) located neurons. In this manner, excitatory cortical connections and a lateral cortical inhibition are modelled (Dominguez et al. 2006; de la Rocha et al. 2008). $V_{r,ij} = \mathrm{sgn}(M(i,j)) \cdot V_r$ denotes the individual reversal potentials, which are calculated from the reversal potential V_r with the use of the sign function of the coupling profile $M(i,j)$: with the considered $V_r = 2$, parameter $V_{r,ij} = 2$ to realize the excitatory interaction and $V_{r,ij} = -2$ to realize the inhibitory interaction.

The normalized sum of the PSPs $s_j(t)$ in Eq. 3 represents the collective synaptic activity of the neuronal population, which yields the *local field potential* $LFP(t) = N^{-1}\sum_{j=1}^{N} s_j(t)$. The LFP will be used to detect synchronization. Low-amplitude LFP oscillations are characteristic for a desynchronized regime (Fig. 1c, red curve). For sufficiently strong synaptic weights the neurons are synchronized, their frequencies $\{\omega_i\}$ are narrowly distributed around the mean $\overline{\omega} \approx 2.73$Hz with standard deviation $\sigma_\omega \approx 0.02$ (Fig. 1b). The neurons burst synchronously, which results in large-amplitude LFP oscillations (Fig. 1d, *red curve*).

We investigate the neuronal population (1)–(3) with *spike timing-dependent plasticity (STDP)* (Gerstner et al. 1996; Markram et al. 1997; Feldman 2000; Wittenberg and Wang 2006; Caporale and Dan 2008). Crucial is the time difference $\Delta t_{ij} = t_i - t_j$, i.e. the time delay between the nearest onsets of the bursts of the pre-synaptic neuron j and the post-synaptic neuron i. Depending on Δt_{ij}, the synaptic weight c_{ij} is updated in a point process-like manner by the increment $0.007\Delta c_{ij}$ for excitatory connections and $-0.007\Delta c_{ij}$ for inhibitory connections according to the rule

$$\Delta c_{ij} = \begin{cases} \mathrm{e}^{-5\Delta t_{ij}/\tau}, & \Delta t_{ij} \geq 0 \\ 5.3\dfrac{\Delta t_{ij}}{\tau}\mathrm{e}^{4\Delta t_{ij}/\tau}, & \Delta t_{ij} < 0 \end{cases}. \quad (4)$$

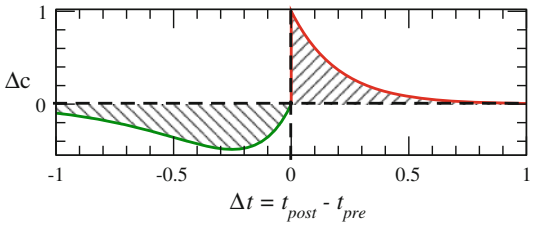

Fig. 2 Normalized plasticity function (Eq. 4 with $\tau = 1$) versus the difference of the burst timing of post- and pre-synaptic neurons $\Delta t = t_{\mathrm{post}} - t_{\mathrm{pre}}$

Owing to STDP (Eq. 4; Fig. 2), the synaptic strength of excitatory synapses is potentiated or depressed depending on whether the post-synaptic firing follows or advances the pre-synaptic firing, respectively (Gerstner et al. 1996; Markram et al. 1997; Debanne et al. 1998; Bi and Poo 1998). For inhibitory or distant synapses, we consider the opposite rule, see (Caporale and Dan 2008) for review. In order to avoid an unbounded growth, the synaptic weights c_{ij} will be confined to the interval $c_{ij} \in [0, c_{\max}]$, where $c_{\max} = 0.5$. The neurons do not have self-connections: $c_{ii} = 0$. As shown theoretically, as an average 'net' effect of STDP, the synaptic weight of excitatory synapses is up-regulated if pre- and post-synaptic neurons preferentially fire in synchrony, whereas it is down-regulated if they fire in an uncorrelated manner, e.g. due to desynchronizing stimulation (see Tass and Majtanik 2006; Hauptmann and Tass 2007). STDP contributes to a self-stabilization of synchronized and desynchronized states (see below).

Depending on the initial conditions for the synaptic weights $\{c_{ij}\}$ of the neuronal ensemble with STDP (Eqs. 1–4) different long-term dynamics emerge. For the numerical simulations, we consider the elements of the synaptic weight matrix $C = \{c_{ij}\}$ initially Gaussian distributed around the mean value c_0 with standard deviation $\sigma_c = 0.005$. Similar results can also be obtained for a broader distribution of $\{c_{ij}\}$. Considering different values of c_0, we found two different limit states characterized by different mean synaptic weights

$$\overline{C}(t) = \frac{1}{N(N-1)}\sum_{i\neq j}^{N}\mathrm{sgn}(M(i,j))c_{ij}(t)$$

and different extents of synchronization as measured by the amplitude of the LFP oscillations (Fig. 3). Since the network contains excitatory and inhibitory connections, we take both types of coupling into account by evaluating the sign function of the coupling profile $M(i,j)$. Then, the synaptic weights of excitatory and inhibitory synapses positively and negatively contribute to the mean synaptic weight $\overline{C}(t)$, respectively. We found that the mean synaptic weight $\overline{C}$ stabilizes at $\overline{C} \approx 0.35$ and -0.12 (Fig. 3a). Strong synchronization, i.e.

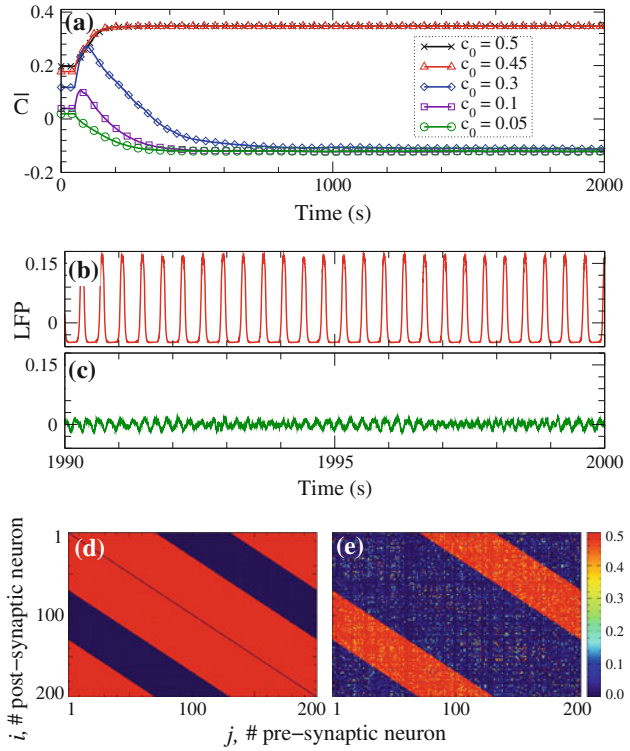

Fig. 3 Multistability in the neuronal ensemble with STDP (Eqs. 1–4). **a** Dynamics of the mean synaptic weight $\overline{C}(t)$ for different initial synaptic weight matrices $C(0) = \{c_{ij}(0)\}$, where $c_{ij}(0)$ are Gaussian distributed with mean values c_0 as indicated in the legend and with standard deviation $\sigma_c = 0.005$. The asymptotic dynamics of the LFP is illustrated for the initial mean synaptic weight $c_0 = 0.45$ in (**b**) and for $c_0 = 0.05$ in (**c**). The corresponding coupling matrices $C = \{c_{ij}\}$ are encoded in colour in plots (**d**) and (**e**), respectively. $\tau = 350$ ms, other parameters as in Fig. 1

high-amplitude LFP oscillations are connected with strong excitatory synaptic weights, whereas weak excitatory and strong inhibitory synaptic weights are connected with desynchronization characterized by low-amplitude fluctuations of the LFP (Fig. 3b, c).

The considered STDP rule (4) leads to interesting structures of the coupling matrix C in the synchronized and desynchronized states (Fig. 3d, e). In the former case, the excitatory synaptic weights are strongly potentiated and the inhibitory synaptic weights are depressed (Fig. 3d), whereas in the latter case the situation is exactly opposite (Fig. 3e). We associate the above synchronized and desynchronized states with regimes of pathological and physiological functionings of the neuronal network, respectively. The pathological state is also characterized by an increased firing rate of the neurons and by an enhancement of the bursting dynamics as found experimentally (Mulders and Robertson 2009; Finlayson and Kaltenbach 2009) and in a modelling study (Houweling et al. 2005). In our model, we also found a statistically significant increase of the firing rate of the neurons in the synchronized state as compared to the desynchronized state. However, the main effect of the up-regulated excitatory synaptic weights is the onset of bursting, where the bursts' size increases on average from nine spikes/burst in the desynchronized state to 17 spikes/burst in the synchronized state (Fig. 1c, d). In this study we however focus on the collective dynamics of the neurons and its control.

In a first approximation, we assume that the neurons of population (1)–(4) receive an afferent input, which we model by Poisson spike trains. External input and stimulation in Eq. 1 read $F_i(t) = F_{i,in}(t) + F_{i,st}(t)$. $F_{i,st}(t)$ is the CR stimulation term (see below). $F_{i,in}(t)$ is the afferent input:

$$F_{i,in}(t) = (V_r - v_i(t)) \cdot \sum_{j=1}^{N} D(i, j, \sigma_p)\eta_j \xi_j(t), \tag{5}$$

where $\xi_j(t)$, $j = 1, 2, \ldots, N$ are independent Poisson spike trains with a mean inter-spike interval (ISI) T_p, and parameter η_j indicates the input strength. At the post-synaptic side of the input neuron, the input spikes are modelled by the $\alpha-$function such that the input spike trains yield

$$\xi_j(t) = \lambda_p(t - t_{k,j})e^{-\lambda_p(t-t_{k,j})}, \; t_{k,j} \le t < t_{k+1,j}, \tag{6}$$

where $\{t_{k,j}\}$ are times of the spike onsets of the j-th spike train, and the ISIs $t_{k+1,j} - t_{k,j}$ are Poisson distributed. The function $D(i, j, \sigma_p)$ defines the spatial profile of the input

$$D(i, j, \sigma_p) = \frac{1}{1 + d_0^2(i - j)^2/\sigma_p^2} \tag{7}$$

implying that the input spike train ξ_j assigned to neuron j influences the neighbouring neurons as well. In this manner, a spatial correlation of the noisy input is introduced. $D(i, j, \sigma_p)$ models the sensitivity of the neurons to input from different afferent fibres, comparable to tuning curves [see, e.g. Refs (Patuzzi and Robertson 1998; Gulick et al. 1989; Robertson and Irvine 1989)]. The above afferent noisy input can have different impacts on the neuronal dynamics and synaptic weights of the target neuronal population depending on its strength. For synchronized neurons, a weak noise does not significantly affect the neuronal dynamics, and the neurons persist to be strongly connected via excitatory synapses and synchronized (Fig. 4a, black curve). On the other hand, stronger input can rewire the network, where the excitatory connections are suppressed, whereas the inhibitory connections are potentiated (Fig. 4a, green curve; compare with Fig. 3a, green curve). As a result, the neurons get desynchronized. However, a noisy input that is too strong can have an opposite effect. For desynchronized neurons with weak excitation and strong inhibition, a strong noisy input increases the relative amount of excitatory coupling among neurons such that, after a short period of administered strong noise (Fig. 4a, red bar), the neuronal population stabilizes at a synchronized state with strong excitation and weak inhibition

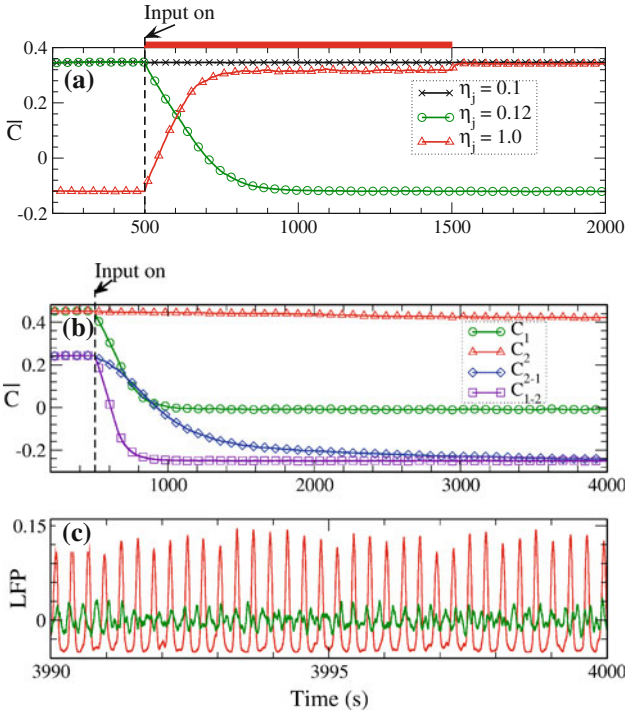

Fig. 4 Impact of the spatially correlated noisy input given by Poisson spike trains on the neuronal population with STDP (1)–(7). **a** Dynamics of the mean synaptic weight $\overline{C}(t)$ for weak and moderate full input administered to synchronized neurons (*black and green curves* for $c_0 = 0.45$) and strong full input administered to desynchronized neurons (*red curve* for $c_0 = 0.05$). The input strengths are indicated in the legend. The input is switched on at 500s. The *upper red bar* denotes the time of the active strong input. **b** Mean synaptic weights of sub-population 1 (C_1, *green curve*) and the deafferented sub-population 2 (C_2, *red curve*) receiving a noisy input of the intensities $\eta_j = 0.12$ and $\eta_j = 0.064$, respectively, administered to the initially synchronized neurons ($c_0 = 0.45$). Mean unidirectional synaptic weights C_{2-1} (2→1, *blue*) and C_{1-2} (1→2, *violet*) between sub-populations. **c** LFP signals of sub-populations 1 (*green*) and 2 (*red*). Parameters $T_p = 230$ ms, $\sigma_p = 0.04$ and $\lambda_p = 24/T_p$. Other parameters as in Fig. 3

(Fig. 4a, red curve; compare with Fig. 3a, red curve). The latter phenomenon can be related to an acoustic trauma (Norena and Eggermont 2006). It eventually leads to the development of a pathological neuronal activity with enhanced neuronal synchronization. In our model, we observe a similar transition. The noise trauma can damage the cochlear such that a neuronal population in the auditory cortex gets partly deafferented and receives a reduced input (Eggermont and Roberts 2004).

Let 50% of the neurons receive the noisy input of full strength, i.e. the complete 'physiological' input. To model the pathologically reduced spontaneous activity of auditory nerve fibres with characteristic frequencies in the hearing loss range (Eggermont 2003), we assume that the other half of the neuronal ensemble is partly deafferented, i.e. it receives only an essentially reduced afferent input, e.g. of about 50% of the full input. To model a circumscribed deafferentation, the $N = 200$ neurons of the entire ensemble are linearly aligned and split into the sub-population 1 (neurons $1, 2, \ldots, 100$) receiving the complete 'physiological' input, and the deafferented sub-population 2 (neurons $101, 102, \ldots, 200$). To illustrate the impact of the input we calculate the mean synaptic weights within sub-population 1 (C_1) and 2 (C_2) and the unidirectional mean synaptic weights from sub-population 1 to sub-population 2 (C_{1-2}) and vice versa (C_{2-1}) (Fig. 4b). The complete ('physiological') input into sub-population 1 causes a depression of its excitatory synaptic weights (Fig. 4b, green curve) and a desynchronized, low-amplitude LFP (Fig. 4c, green curve). Due to the ('pathologically') reduced input the up-regulated connectivity (Fig. 4b, red curve) and synchrony (Fig. 4c, red curve) remain preserved within sub-population 2. Additionally, the synchronized sub-population 2 and the desynchronized sub-population 1 demonstrate a well-pronounced inhibitory interaction by a continuously up-regulated bidirectional inhibitory pathway (negative C_{2-1} and C_{1-2}, Fig. 4b, blue and violet curves).

3 CR stimulation

We apply CR stimulation (Tass 2003b,a) to the neuronal population (1)–(7) from Fig. 4b, c to study whether CR stimulation may counteract the deafferentation-induced up-regulation of both synchrony and connectivity. For this, we employ acoustic CR stimulation. The stimulation signals arrive at the neuronal target population as PSPs, which we model by the α-function of the form (6) with parameter λ_s and the stimulation onset times t_k. According to the CR stimulation algorithm (Tass 2003b,a) the stimulation pulses (in our case in the form of α-functions (6)) are sequentially delivered to M different sub-populations of the neuronal target ensemble (e.g. via M different stimulation sites, see also the discussion in Sect. 4) with a delay of T_s/M between subsequent pulse onsets. We choose $M = 4$ (see Tass 2003b,a). The stimulation period T_s is optimally chosen close to the mean period of the synchronized neurons. Within one cycle of length T_s each stimulation site is activated once. With this, the second (stimulation) component of the input term $F_i(t)$ in Eq. 1 reads

$$F_{i,st}(t) = (V_r - v_i(t)) \cdot K \sum_{j=1}^{M} D(i, x_j, \sigma_s)\rho_j(t)P(t). \quad (8)$$

K is the stimulation strength, $D(i, x_j, \sigma_s)$ is the spatial profile of the stimulation strength, decaying with distance between the stimulation site j with lattice coordinate x_j and neuron i. We consider a quadratic spatial decay profile (7). This type of spatial decay profile is characteristic for electrical stimulation of brain tissue (Richardson et al. 2003) and also fits to the frequency characteristics of tuning curves (Patuzzi and Robertson 1998; Gulick et al. 1989; Robertson and Irvine

1989). $\rho_j(t)$ is an indicator function controlling the activation of the stimulation site j, and $P(t)$ is a periodic α-train of the form (6) (see also (Popovych and Tass 2011)) with the stimulation onset times t_k such that $t_{k+1} - t_k = T_s/M$.

The indicator function $\rho_j(t)$ in Eq. 8 equals 1 if the jth stimulation site is active at time t and zero otherwise. The switching times correspond to the stimulation onset times t_k of the α-train P. We apply CR stimulation, where the sequence of stimulation site activation is randomly varied between cycles with equal probability. To exploit the transient desynchronization induced by CR stimuli (Tass 2003b,a), we use a patterned n cycles ON, m cycles OFF protocol (with cycle duration T_s, and $m = 3$, $n = 3$), where CR stimulation is delivered only during the ON cycles, and desynchronization is strongest during the OFF cycles.

The neuronal population (1)–(8) comprises sub-population 1, which receives 'physiological' afferent input, and the partly deafferented sub-population 2, which receives 'pathologically' reduced input. Without CR stimulation, neurons within sub-populations 1 and 2 are desynchronized and synchronized, respectively (Fig. 4b, c), where the excitatory intra-population couplings are down- and up-regulated, correspondingly (Fig. 5c). We deliver CR stimulation via equally spaced stimulation sites, two located in both sub-populations such that the four stimulation sites are located at lattice coordinates $x_j = 25, 75, 125, 175$. The synaptic weights within sub-population 2 are down-regulated by CR stimulation and finally relaxed to zero after CR offset (Fig. 5a, red curve and Fig. 5d). During CR stimulation, the unidirectional couplings between sub-populations 1 and 2 are not significantly influenced. CR stimulation induces a slight transient increase of the internal coupling within sub-population 1, which fades away after CR offset (Fig. 5a, green curve and Fig. 5d).

In the stimulation set-up of Fig. 5a, b, we delivered the CR stimuli widespread over the whole neuronal population. One might wonder whether the transient up-regulation of the synaptic weight in sub-population 1 can still be observed if we deliver the CR stimuli selectively to the deafferented sub-population (ranging from lattice coordinates $x_j = 101$ to 200) only. Accordingly, in Fig. 5e, we administer the CR stimuli to the deafferented sub-population, at lattice coordinates $x_j = 112, 137, 163, 188$. In this case, we achieve an anti-kindling, too: After CR stimulation offset, both sub-populations get desynchronized (with LFPs as in Fig. 5b), and the connectivity within the sub-populations vanishes (Fig. 5e). There is no transitory increase of the connectivity in the normal sub-population (C_1) during CR stimulation (Fig. 5e, green curve), since the latter is not directly stimulated as in the widespread set-up from Fig. 5a. Moreover, CR stimulation gets even more effective, where the internal coupling within sub-population 2 is down-regulated much faster (Fig. 5e, red curve). Hence, our simulations suggest that it is beneficial to deliver CR stimulation to the deafferented region only.

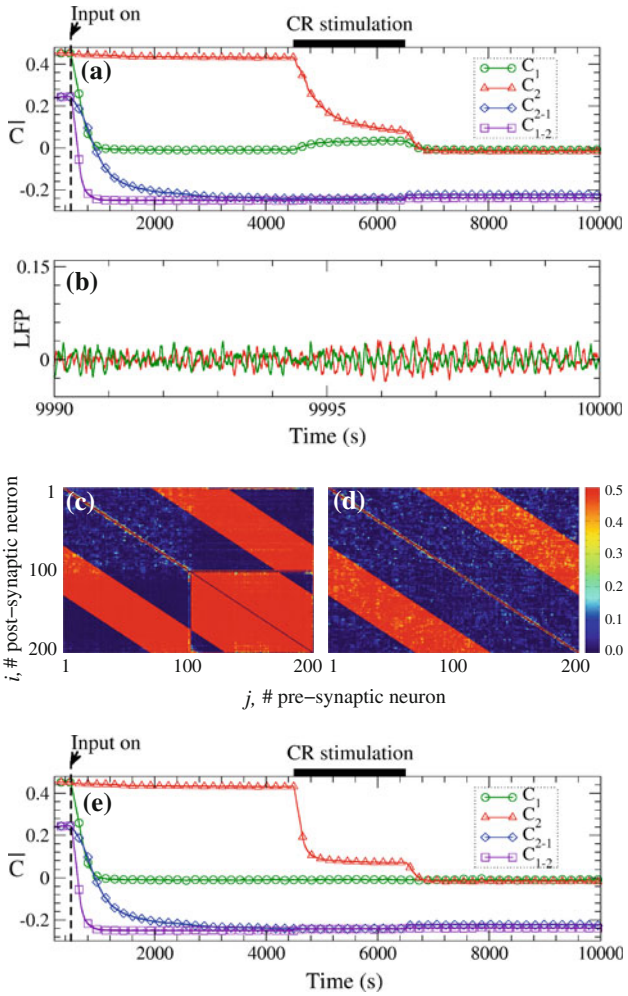

Fig. 5 **a–d** CR stimulation of the population from Fig. 4b, c with CR stimuli delivered to both the deafferented and the normal sub-population (at lattice coordinates $x_j = 25, 75, 125, 175$). **a** Mean synaptic weights C_1 and C_2 of sub-populations 1 and 2, respectively, and mean unidirectional synaptic weights C_{2-1} (2→1) and C_{1-2} (1→2) between sub-populations as indicated in the legend. CR epoch indicated by horizontal black bar. **b** LFP signals of sub-populations 1 (*green*) and 2 (*red*). **c, d** Coupling matrices $C = \{c_{ij}\}$ are encoded in color for the states **c** just before the onset of CR stimulation at $t = 4500$ s and **d** after a post-stimulation transient at $t = 10000$ s. **e** CR stimulation of the population from Fig. 4b, c with CR stimuli exclusively delivered to the deafferented sub-population (at $x_j = 112, 137, 163, 188$). Same format as in **a**. CR parameters: $K = 0.24$, $\sigma_s = 0.5$, $T_s = 300$ ms, and $\lambda_s = 4M/T_s$ for the α-train $P(t)$ of the form (6). Other parameters as in Fig. 4

The tinnitus pitch is localized within the frequency range of the deafferented sub-population (Eggermont and Roberts 2004). Interestingly, our computational results discussed above correlate with the findings of a modelling study and a clinical pilot study (Schaette and Kempter 2006; Schaette et al. 2010) showing that acoustic stimulation with hearing aids or noise devices are most effective if the stimulation frequencies well overlap with the tinnitus frequency.

To compare the efficacy of CR stimulation in rewiring and desynchronization of abnormally coupled and synchronized neuronal networks to, for example, broad-band noisy input, we calculate the amount of administered current into the neuronal population for the cases of sensory CR stimulation and weakly spatially correlated Poisson noisy input (Fig. 4a, green curve). For this, we average the administered stimulation current from Eq. 8 and the input current from Eq. 5 over the network and over time such that the average amount of the current received by a single neuron per time unit can be calculated. We found that for the considered parameters, effective CR stimulation needs about four times less current than the effective noisy input. Moreover, CR stimulation is definitely more robust with respect to a variation of the stimulation intensity than the noisy input. We have verified that CR stimulation can effectively rewire and desynchronize the stimulated network even if the stimulation strength K is increased by 25 times (not shown). On the other hand, the noisy input can induce an up- and down-regulation of the excitatory and inhibitory synaptic weights, respectively, and can boost synchronization if its intensity is increased by a factor 8 (Fig. 4a, compare green and red curves). These calculations suggest that acoustic CR stimulation can be a good candidate for a reliable control of synchronization and abnormal interactions in affected neuronal populations.

4 Acoustic coordinated reset stimulation

CR stimulation has been suggested in Refs. (Tass 2003b,a) for the control of abnormal neuronal synchronization by electrical stimulation, where brief trains of high-frequency electrical pulses are administered to the neuronal tissue. Electrical CR stimulation would however require an electrode implantation into the central auditory system. We here sketch a possible alternative, a non-invasive approach which employs the tonotopic organization of the auditory cortex. In our model (Eqs. 1–8), we considered an acoustic CR stimulation, where the target neurons receive the stimulation signals in the form of PSPs generated in their dendrites in response to peripheral acoustic stimuli. In terms of our model, tonotopic organization means that the neurons respond to sounds of different frequencies, where the latter, e.g. increase with increasing lattice coordinate x_j. We replace electrical stimulation at different sites by an application of brief pure tones of different pitch (e.g. originating from a sound generator and delivered via headphones) to stimulate neuronal sub-populations at different tonotopically defined sites. Instead of a brief electrical pulse train (Tass 2003b,a), we deliver a brief tone (consisting of a sine wave multiplied by a smooth envelope). To realize a four-site CR stimulation, we choose $M = 4$ tones of different pitches and deliver them with a delay of T_s/M in between subsequent tone onsets. The stimulation period (cycle) T_s should optimally correspond to the mean period of the pathological rhythm (Tass 2003b,a), i.e. the delta EEG rhythm in temporal regions (Weisz et al. 2005, 2007). However, the effect of CR stimulation is robust with respect to variations of the cycle duration T_s relative to the mean period of the pathological rhythm (Tass 2003b,a), and hence, one can just choose T_s to correspond to the delta frequency range, without any calibration and without electrophysiological (e.g. EEG) recordings. An open loop setup is attractive given its non-invasiveness and clinical feasibility. Between cycles the sequence of pitches is randomly varied with equal probability.

The pitches of the CR tones should be grouped around the patient-specific tinnitus frequency to make sure that the CR tones reach the pathologically synchronized region. Note that in our simple model, CR is effective no matter whether we confine the CR stimuli to the deafferented region (Fig. 5e) or stimulate both the deafferented and the non-deafferented regions (Fig. 5a, b). Whether this holds also in patients remains to be verified. For this purpose, in patients, the deafferented region can be assessed audiometrically. The proper spacing of pitches of the different CR tones should be optimal in the following sense: (i) Because of the overlapping frequency response properties of central auditory neurons given by the tuning curves, the spacing should not be too narrow to ideally stimulate distinct sub-populations with the different CR tones; (ii) The spacing should not be too wide since it should primarily affect the deafferented region. For this strategy, acoustic CR stimulation requires a sufficient residual hearing ability in the deafferented region (or appropriate support by hearing aids or cochlear implants).

The electrical pulse train of electrical CR stimulation resets the phase of the stimulated sub-population (Tass 2003b,a). This is achieved either by a strong burst (hard reset), or by delivering a few, say three, weaker bursts within three ON cycles (soft reset, see Tass 2002) in the 3 cycles ON, 3 cycles OFF protocol (see Sect. 3). By the same token, auditory tone stimuli may induce phase resets (see Klimesch et al. 2006). In our model, we show that CR stimulation remains to be effective if the electrical high-frequency pulse trains are replaced by α-trains modelling the PSPs, which thus supports the application of CR stimulation algorithm to acoustic stimulation.

5 Discussion

During the past few decades, increasing attention has been paid to the modelling of the development of pathological neuronal activity in the auditory system following deafferentation. In several studies, the contributions of different pathophysiological mechanisms to the emergence of tinnitus-associated pathological dynamics have been analysed. Lateral inhibition has been hypothesized to play an important

role in the emergence of tinnitus at the audiometric edge of the hearing loss (Gerken 1996). An increase of the response gain of central auditory neurons after hearing loss can amplify internal noise and elevate spontaneous firing rates of the neurons leading to a perception of a phantom sound (Parra and Pearlmutter 2007). The up-regulation of excitation and down-regulation of inhibition due to cortical homeostatic plasticity can provide a modelling approach which well reproduces tinnitus-related neuronal activity, which reveals an increase of spontaneous neuronal firing and an enhancement of neuronal synchrony (Houweling et al. 2005; Schaette and Kempter 2006; Dominguez et al. 2006), and predicts the tinnitus pitch from the audiograms of tinnitus patients (Schaette and Kempter 2009).

The simple dynamical model considered in the present study includes STDP in an explicit form, which intelligibly depends on the underlying neuronal activity. Our model still captures many key features of the pathological tinnitus-related neuronal activity. In particular, the model shows an enhancement of neuronal synchrony and bursting in the pathological state which emerges in response to a strong noisy input modelling the effect of a noise trauma. Governed by STDP the excitatory and inhibitory synaptic connections are up- and down-regulated, respectively, which serves as a mechanism for the onset of the abnormal neural synchrony. If the noise trauma is followed by a partial deafferentiation of the affected neuronal population, then the latter splits into two sub-populations, one being weakly synchronized, with physiological synaptic connections, the other, deafferented one being strongly synchronized, with up-regulated synaptic weights.

Moreover, we also observe that if the deafferented neuronal sub-population receives a permanent noisy input of appropriate strength, then it may prevent from the emergence of pathological synchrony (Fig. 4a, green curve). This effect is in accordance with experimental findings in cat auditory cortex, where cats, placed in a high-frequency-enriched acoustic environment after a noise trauma, did not show significant differences in neuronal synchrony and firing rates compared to controls (Norena and Eggermont 2006). However, as shown in Sect. 3, if the noisy input gets stronger, then it induces an opposite effect and leads to kindling and synchronization. In contrast, in our model, CR stimulation is effective for a considerably larger range of the stimulation amplitude (see Sect. 3).

Illustrated by numerical simulations of the above model, we sketched a novel, non-invasive approach, acoustic CR stimulation, to counteract pathological synchrony and connectivity in the central auditory system underlying subjective tonal tinnitus (Dohrmann et al. 2007; Kahlbrock and Weisz 2008; De Ridder et al. 2011). Previously, it was shown that electrical CR stimulation robustly causes an anti-kindling in different networks with and without inhibition, but without afferent input (Tass and Majtanik 2006; Tass and Hauptmann 2007, 2009; Hauptmann and Tass 2007). In the present study, our simulations are intended to illustrate the concept of CR-induced anti-kindling for the therapy of tinnitus. Of course, safety and efficacy of acoustic CR stimulation have to be studied in a controlled clinical trial.

The contact sequence for CR was randomized (Sect. 3) to prevent from reverberations and, hence, possible maladaptive synaptic learning, hindering the desired anti-kindling. However, probably due to its strong desynchronizing effect, CR with fixed stimulation contact sequence revealed practically the same results (data not shown).

Acknowledgements This study was supported by the Network of Excellence in Biosimulation (BioSim LSHB-CT-20004-005137).

References

Baer SM, Gaekel EM (2008) Slow acceleration and deacceleration through a hopf bifurcation: power ramps, target nucleation, and elliptic bursting. Phys Rev E 78(3):036205

Bauer CA, Turner JG, Caspary DM, Myers KS, Brozoski TJ (2008) Tinnitus and inferior colliculus activity in chinchillas related to three distinct patterns of cochlear trauma. J Neurosci Res 86(11):2564–2578

Bi GQ, Poo MM (1998) Synaptic modifications in cultured hippocampal neurons: dependence on spike timing, synaptic strength, and postsynaptic cell type. J Neurosci 18:10464–10472

Calford M, Rajan R, Irivine D (1993) Rapid changes in the frequency tuning of neurons in cat auditory cortex resulting from pure-tone induced temporary threshold shift. J Neurosci 55:953–964

Caporale N, Dan Y (2008) Spike timing-dependent plasticity: a hebbian learning rule. Annu Rev Neurosci 31:25–46

Debanne D, Gahweiler B, Thompson S (1998) Long-term synaptic plasticity between pairs of individual CA3 pyramidal cells in rat hippocampus slice cultures. J Physiol 507:237–247

de la Rocha J, Marchetti C, Schiff M, Reyes AD (2008) Linking the response properties of cells in auditory cortex with network architecture: cotuning versus lateral inhibition. J Neurosci 28(37):9151–9163

De Ridder D, van der Loo E, Vanneste S, Gais S, Plazier M, Kovacs S, Sunaert S, Menovsky T, van de Heyning P (2011) Theta-gamma dysrhythmia and auditory phantom perception case report. J Neurosurg 114(4):912–921

Dohrmann K, Elbert T, Schlee W, Weisz N (2007) Tuning the tinnitus percept by modification of synchronous brain activity. Restor Neurol Neurosci 25:371–378

Dominguez M, Becker S, Bruce I, Read H (2006) A spiking neuron model of cortical correlates of sensorineural hearing loss: spontaneous firing, synchrony, and tinnitus. Neural Comput 18(12):2942–2958

Eggermont J (2003) Central tinnitus. Auris Nasus Larynx 30:S7–S12

Eggermont J, Roberts L (2004) The neuroscience of tinnitus. Trends Neurosci 27:676–682

Elbert T, Flor H, Birbaumer N, Knecht S, Labrig W, Taub E (1994) Extensive reorganization of the somatosensory cortex in adult humas after nervous system injury. Neuroreport 5:2593–2597

Feldman DE (2000) Timing-based LTP and LTD at vertical inputs to layer II/III pyramidal cells in rat barrel cortex. Neuron 27(1): 45–56

Finlayson PG, Kaltenbach JA (2009) Alterations in the spontaneous discharge patterns of single units in the dorsal cochlear nucleus following intense sound exposure. Hear Res 256(1-2):104–117

Flor H, Elbert T, Knecht S, Wienbruch C, Pantev C, Birnbaumer N, Larbrig W, Taub E (1995) Phantom-limb pain as a perceptual correlate of cortical reorganization following arm amputation. Nature 375:482–484

Gerken GM (1996) Central tinnitus and lateral inhibition: an auditory brainstem model. Hear Res 97(1-2):75–83

Gerstner W, Kistler WM (2002) Spiking neuron models: single neurons, populations, plasticity. Cambridge University Press, Cambridge

Gerstner W, Kempter R, van Hemmen J, Wagner H (1996) A neuronal learning rule for sub-millisecond temporal coding. Nature 383:76–81

Golomb D, Rinzel J (1993) Dynamics of globally coupled inhibitory neurons with heterogeneity. Phys Rev E 48:4810–4814

Gulick W, Gescheider G, Frisina R (1989) Hearing: physiological acoustics, neural coding, and psychoacoustics. Oxford University Press, Oxford

Hauptmann C, Tass PA (2007) Therapeutic rewiring by means of desynchronizing brain stimulation. Biosystems 89:173–181

Heller AJ (2003) Classification and epidemiology of tinnitus. Otolaryngol Clin N Am 36:239–248

Houweling AR, Bazhenov M, Timofeev I, Steriade M, Sejnowski TJ (2005) Homeostatic synaptic plasticity can explain post-traumatic epileptogenesis in chronically isolated neocortex. Cereb Cortex 15(6):834–845

Irvine D, Rajan R, Brown M (2001) Injury- and use-related plasticity in adult auditory cortex. Audiol Neurootol 6:192–195

Izhikevich EM (2001) Synchronization of elliptic bursters. SIAM Rev 43:315–344

Izhikevich EM (2007) Dynamical systems in neuroscience: the geometry of excitability and bursting. MIT Press, Cambridge

Jastreboff PJ (1990) Phantom auditory perception (tinnitus): mechanisms of generation and perception. Neurosci Res 8:221–254

Kahlbrock N, Weisz N (2008) transient reduction of tinnitus intensity is marked by concomitant reductions of delta band power. BMC Biol 6:4

Klimesch W, Hanslmayr S, Sauseng P, Gruber W (2006) Distinguishing the evoked response from phase reset: A comment to mäkinen et al. Neuroimage 29:808–811

Markram H, Lübke J, Frotscher M, Sakmann B (1997) Regulation of synaptic efficacy by coincidence of postsynaptic aps and epsps. Science 275:213–215

McFadden D (1982) Tinnitus: facts, theories, and treatments. National Academies Press, Washington, DC

Mühlnickel W, Elbert T, Taub E, Flor E (1998) Reorganization of auditory cortex in tinnitus. Proc Natl Acad Sci USA 95:10340–10343

Mulders WHAM, Robertson D (2009) Hyperactivity in the auditory midbrain after acoustic trauma: dependence on cochlear activity. Neuroscience 164(2):733–746

Norena AJ, Eggermont JJ (2003) Changes in spontaneous neural activity immediately after an acoustic trauma: implications for neural correlates of tinnitus. Hear Res 183(1-2):137–153

Norena AJ, Eggermont JJ (2006) Enriched acoustic environment after noise trauma abolishes neural signs of tinnitus. Neuroreport 17(6):559–563

Ortmann M, Muller N, Schlee W, Weisz N (2011) Rapid increases of gamma power in the auditory cortex following noise trauma in humans. Eur J Neurosci 33(3):568–575

Parra LC, Pearlmutter BA (2007) Illusory percepts from auditory adaptation. J Acoust Soc Am 121(3):1632–1641

Patuzzi R, Robertson D (1988) Tuning in the mammalian cochlea. Physiol Rev 68(4):1009–1082

Popovych OV, Tass PA (2011) Macroscopic entrainment of periodically forced oscillatory ensembles. Prog Biophys Mol Biol 105:98–108

Rajan R, Irvine D (1998) Neuronal responses across cortical field a1 in plasticity induced by peripheral auditory organ damage. Audiol Neurootol 3:123–144

Richardson KA, Gluckman BJ, Weinstein SL, Glosch CE, Moon JB, Gwinn RP, Gale K, Schiff SJ (2003) In vivo modulation of hippocampal epileptiform activity with radial electric fields. Epilepsia 44(6):768–777

Rinzel JA (1987) A formal classification of bursting mechanisms in excitable systems. In: Teramoto E, Yamaguti M (eds) Mathematical topics in population biology, morphogenesis and neurosciences, lecture notes in biomathematics 71. Springer-Verlag, New York, pp 267–281

Robertson D, Irvine DRF (1989) Plasticity of frequency organization in auditory-cortex of guinea-pigs with partial unilateral deafness. J Comp Neurol 282(3):456–471

Schaette R, Kempter R (2006) Development of tinnitus-related neuronal hyperactivity through homeostatic plasticity after hearing loss: a computational model. Eur J Neurosci 23:3124–3138

Schaette R, Kempter R (2009) Predicting tinnitus pitch from patients' audiograms with a computational model for the development of neuronal hyperactivity. J Neurophysiol 101(6):3042–3052

Schaette R, Konig O, Hornig D, Gross M, Kempter R (2010) Acoustic stimulation treatments against tinnitus could be most effective when tinnitus pitch is within the stimulated frequency range. Hear Res 269(1-2):95–101

Steriade M (2006) Grouping of brain rhythms in corticothalamic systems. Neuroscience 137:1087–1106

Tass P (2002) Desynchronization of brain rhythms with soft phase-resetting techniques. Biol Cybern 87:102–115

Tass P, Hauptmann C (2007) Therapeutic modulation of synaptic connectivity with desynchronizing brain stimulation. Int J Psychophysiol 64:53–61

Tass P, Silchenko A, Hauptmann C, Barnikol U, Speckmann EJ (2009) Long-lasting desynchronization in rat hippocampal slice induced by coordinated reset stimulation. Phys Rev E 80:011902

Tass PA (2003) Desynchronization by means of a coordinated reset of neural sub-populations—a novel technique for demand-controlled deep brain stimulation. Prog Theor Phys Suppl 150:281–296

Tass PA (2003) A model of desynchronizing deep brain stimulation with a demand-controlled coordinated reset of neural subpopulations. Biol Cybern 89:81–88

Tass PA, Hauptmann C (2009) Anti-kindling achieved by stimulation targeting slow synaptic dynamics. Restor Neurol Neurosci 27(6):589–609

Tass PA, Majtanik M (2006) Long-term anti-kindling effects of desynchronizing brain stimulation: a theoretical study. Biol Cybern 94(1):58–66

Terman D, Rubin JE, Yew AC, Wilson CJ (2002) Activity patterns in a model for the subthalamopallidal network of the basal ganglia. J Neurosci 22(7):2963–2976

Weisz N, Moratti S, Meinzer M, Dohrmann K, Elbert T (2005) Tinnitus perception and distress is related to abnormal spontaneous brain activity as measured by magnetoencephalography. PLOs Med 2:e153

Weisz N, Hartmann T, Dohrmann K, Schlee W, Norena A (2006) High-frequency tinnitus without hearing loss does not mean absence of deafferentation. Hear Res 222:108–114

Weisz N, Mueller S, Schlee W, Dohrmann K, Hartmann T, Elbert T (2007) The neural code of auditory phantom perception. J Neurosci 27:1479–1484

Wittenberg GM, Wang SSH (2006) Malleability of spike-timing-dependent plasticity at the CA3–CA1 synapse. J Neurosci 26(24):6610–6617

Yuste R, Bonhoeffer T (2004) Genesis of dendritic spines: insights from ultrastructural and imaging studies. Nat Rev Neurosci 5:24–34